Preprints of the 19th World Congress
The International Federation of Automatic Control
Cape Town, South Africa. August 24-29, 2014

Wind turbine blade flapwise vibration control through input shaping

Dayuan Ju*. Qiao Sun.**

**Mechanical and Manufacturing Engineering Department, University of Calgary, Calgary,Alberta,Canada,(dju@ucalgary.ca)*
*** Mechanical and Manufacturing Engineering Department, University of Calgary, Calgary,Alberta,Canada,(qsun@ucalgary.ca)*

Abstract: Wind turbine blade vibration is a serious problem not only because it will reduce the life of blade but also can it pass some unexpected frequencies to the tower, which will cause tower to vibrate. The aim of this paper is to develop a model for wind turbine flapwise vibration and reduce the pitch angle caused vibrations in flapwise direction. Lagrange's method is used to model the blade and input shaping method is used to reduce the residual vibrations caused by the change of pitch angle input. Effectiveness of designed input shaper is verified through comparison.

Keyword: vibration control; modeling; feedforward control; input shaping; wind turbine blade; flapwise deflection; pitch angle

1. INTRODUCTION

Wind turbine mechanical vibrations can pose some potential threat to the environment, not only can it be harmful to living lives, it may destroy the fundamental structure of terrain over considerable distances as well. Among all the mechanical vibrations in wind turbine, blade vibrations can be of great significance because blades are the first mechanical part of wind turbine that interacts with wind and play a key role in wind power generation. Also, there's a dynamic interaction between wind turbine blades and tower, meaning that tower motion is connected to the motion of blades. Therefore, the suppression of wind turbine blade vibration is important.

Researchers have developed several ways to reduce the vibration of wind turbine blade. John Arrigan studied the potential of using semi-active tuned mass dampers to reduce vibrations in the flapwise direction with changing parameters in the wind turbine. By doing the numerical simulations, they verified the effectiveness of this method. Victor Maldonaldo and John Farnsworth investigated the feasibility of using synthetic jet actuators to enhance the performance of wind turbine blade vibration reduction. The key idea of using this technique is to change the air flow field over the blade so the aerodynamic properties of the blade are altered. Recently, smart turbine blades are developed to reduce the loads on blade.

Although researchers have developed many ways to suppress blades vibrations over the years, none of them explored the effect of fast pitch rates on the blade. Normally, when the pitch rates are fast, the pitch angle input can be considered as step input, this, of course, will cause some additional vibrations to the blades. In this paper, the effects of fast pitch rates on wind turbine blade flapwise deflection is analyzed and input shaping method is used to reduce blade flapwise deflection.

There are many papers about wind turbine modeling and most of them are developed for power generation purpose. To analyze the flapwise deflection of wind turbine blade, a model for vibration purpose is developed in this paper with only flapwise deflection considered. Here, we consider wind turbine blade as a cantilever beam with one side fixed and the other side free to move. The effect of rotating, which is centrifugal stiffening, is also taken into account.

This paper is organized as follow. In section 2, we explain the model of flapwise displacement of wind turbine blade we developed. In section 3, theory about input shaping is introduced and a suitable input shaping method is designed. In section 4, we analyze the model developed in this paper and compare the result of blade flapwise deflection when there's no input shaping and when input shaper is added. Finally, discussions and conclusions are given in section 5.

2. MODELING OFWIND TURBINE BLADE

2.1 Coordinate transformation

Fig 1 is nacelle coordinate, which is fixed on the nacelle and could be considered as inertial reference frame. Subscript "N" is used to identify nacelle coordinate. Fig 2 is hub coordinate which rotates with the rotor, but this coordinate does not pitch with blade and subscript "h" is used to identify it. The relationship between this two coordinates is show in Fig 3, from which we can see that the difference between this two coordinates is the azimuth angle Ψ. Fig 4 shows the blade coordinate and its relationship with hub coordinate. In the blade coordinate, $\vec{z}_b$ axis is pointing along the pitch axis towards the tip of blade and $\vec{y}_b$ axis is pointing towards the trailing edge of blade. $\vec{x}_b$ axis is orthogonal with $\vec{y}_b$ axis and $\vec{z}_b$ axis such that they form a right-hand coordinate. Z axis of hub coordinate coincides with z axis of blade coordinate.

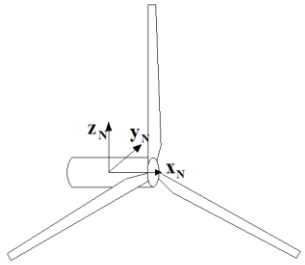

Fig1. Nacelle coordinate

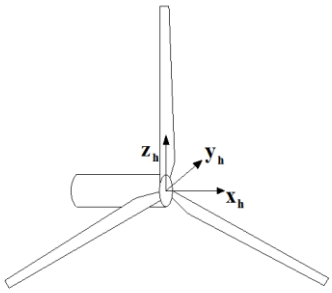

Fig2. Hub coordinate

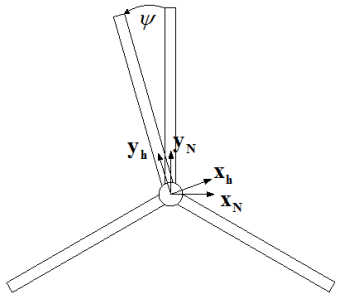

Fig3.Nacelle and Hub coordinate

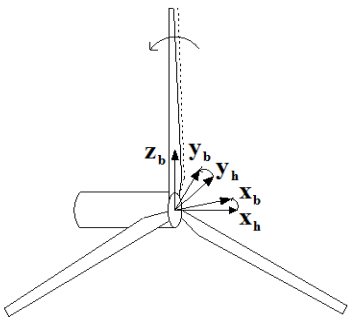

Fig4. Blade coordinate

The relationship between these coordinates can be described as

$$\begin{bmatrix} \mathbf{x_N} \\ \mathbf{y_N} \\ \mathbf{z_N} \end{bmatrix} = \begin{bmatrix} 1 & 0 & 0 \\ 0 & \cos\psi & -\sin\psi \\ 0 & \sin\psi & \cos\psi \end{bmatrix} \begin{bmatrix} \mathbf{x_h} \\ \mathbf{y_h} \\ \mathbf{z_h} \end{bmatrix} \quad (1)$$

$$\begin{bmatrix} \mathbf{x_h} \\ \mathbf{y_h} \\ \mathbf{z_h} \end{bmatrix} = \begin{bmatrix} \cos\theta & -\sin\theta & 0 \\ \sin\theta & \cos\theta & 0 \\ 0 & 0 & 1 \end{bmatrix} \begin{bmatrix} \mathbf{x_b} \\ \mathbf{y_b} \\ \mathbf{z_b} \end{bmatrix} \quad (2)$$

2.2 Kinetic and potential energy

Blade is modeled as a uniform rotating cantilever Euler-Bernoulli beam with no mass fixed at the tip and assumed mode method is used to determine blade flapwise deflection. With this technique, blade is modeled as a linear sum of known mode shapes and dominant normal vibration modes. The flapwise deflection of the blade under this method can be expressed as

$$y_f(x,t) = \sum_{i=1}^{n} \phi_i(x) q_i(t) \quad (3)$$

where y_f is the blade flapwise displacement, $\emptyset_i$ is the mode shape function and q_i is generalized coordinate. Although cantilever beam has many vibrations modes, only the first two modes are considered since the first two has the most dominant influences on beam's vibration.
According to Bramwell, the effect of rotation of a blade on mode shapes and natural frequency is quite small; therefore the non-rotating mode shapes can be served as approximations in the calculation of the rotating modes. The mode shape function we choose here is:

$$\phi_n = \cosh\beta_n x - \cos\beta_n x - \alpha_n(\sinh\beta_n x - \sin\beta_n x) \quad (4)$$

where β_n and α_n are some characteristic parameters, their values can be found from reference book.

Assuming P is a point on the blade, when the blade is rotating, the speed of point P can be expressed as

$$\mathbf{v_p} = -(r_{hub} + x)\omega \mathbf{j_h} + \frac{\partial y_f(x,t)}{\partial t}\mathbf{i_b} - y_f \omega \mathbf{k_b} \quad (5)$$

where r_{hub} is the hub radius, x is the distance along the flexible blade, ω is the rotor speed, $\vec{\mathbf{j}}_\mathbf{h}$ is unit vector in $\vec{\mathbf{y}}_\mathbf{h}$ direction, $\vec{\mathbf{i}}_\mathbf{b}$ is unit vector in $\vec{\mathbf{x}}_\mathbf{b}$ direction, $\vec{\mathbf{k}}_\mathbf{b}$ is unit vector in $\vec{\mathbf{z}}_\mathbf{b}$ direction. The last term in equation (5) is axial velocity.

From the coordinate transformation we have

$$\mathbf{j_h} = \sin\theta \mathbf{i_b} + \cos\theta \mathbf{j_b} \quad (6)$$

Therefore, the expression for the blade kinetic energy can be written as

$$T = \frac{1}{2} m\omega^2 \int_0^L (r_{hub} + x)^2 dx + \frac{1}{2} m \dot{\mathbf{q}}^{\mathrm{T}} \mathbf{M} \dot{\mathbf{q}} - m\omega \boldsymbol{\Phi} \cdot \dot{\mathbf{q}} + \frac{1}{2} m\omega^2 \mathbf{q}^{\mathrm{T}} \mathbf{M} \mathbf{q} \quad (7)$$

where $$\mathbf{M}_{ij} = \int_0^L \phi_i(x)\phi_j(x)dx \quad (8)$$

$$\mathbf{\Phi}_i = \int_0^L (r_{hub} + x)\sin\theta\phi_i(x)dx \qquad (9)$$

The potential energy consists of three parts: potential energy associated with the distributed flap-wise stiffness of the beam, potential energy associated with centrifugal force and potential energy associated gravity:

$$V = V_{strain} + V_{rotation} + V_{gravity} \qquad (10)$$

The potential energy associated with strain can be expressed as

$$V_{strain} = \frac{1}{2}\int_0^L EI\left[\frac{\partial^2 y(x,t)}{\partial x^2}\right]^2 dx = \frac{1}{2}EI\mathbf{q}^T\mathbf{K}\mathbf{q} \qquad (11)$$

where $$\mathbf{K} = \int_0^L \frac{d^2\phi_i(x)}{dx^2}\frac{d^2\phi_j(x)}{dx^2}dx \qquad (12)$$

and EI is the blade flapwise distributed stiffness.

The potential energy associated with centrifugal force can be expressed as:

$$V_{centrifugal} = \int_0^L m\cdot\omega^2\cdot x\cdot v(x,t)dx = \frac{1}{2}m\omega^2\mathbf{q}^T\mathbf{I}\mathbf{q} \qquad (13)$$

where $$\mathbf{I} = \int_0^L x(\int_0^x \frac{d\phi_i(\bar{x})}{d\bar{x}}\frac{d\phi_j(\bar{x})}{d\bar{x}}d\bar{x})dx \qquad (14)$$

and $v(x,t)$ is the axial displacement caused by centrifugal force.

The potential energy caused by gravity is

$$\begin{aligned} V_{gravity} &= -mg\sin\psi\sin\theta\cdot\frac{1}{2}\int_0^L y_f dx \\ &= -\frac{1}{2}mg\sin\psi\sin\theta\cdot\mathbf{q}^{\mathbf{T}}\mathbf{M}\mathbf{q} \end{aligned} \qquad (15)$$

Therefore the total potential energy is

$$\begin{aligned} &V = V_{strain} + V_{centrifugal} + V_{gravity} = \\ &\frac{1}{2}EI\mathbf{q}^T\mathbf{K}\mathbf{q} + \frac{1}{2}m\omega^2\mathbf{q}^T\mathbf{I}\mathbf{q} - \frac{1}{2}mg\sin\psi\sin\theta\cdot\mathbf{q}^{\mathbf{T}}\mathbf{M}\mathbf{q} \end{aligned} \qquad (16)$$

2.3 Aerodynamics

Blade element theory is used to analyze blade aerodynamics. Fig 5 shows blade element theory geometry on a blade transversal section. When airflow establishes a differential pressure around the blade element, two forces will be resulted, lift force and drag force. Lift force is perpendicular to the local incoming flow stream and drag force is parallel to the flow direction. Usually, another two forces are used in the analysis of aerodynamics as an alternative of lift force and drag force, which is, normal force and tangential force. Normal force is perpendicular to the chord line and tangential force is parallel to the chord line. Since flapwise deflection of the blade is perpendicular to the chord line of the blade, thus normal force should be responsible for the blade flapwise displacement. In Fig 5, θ is airflow angle, which is the angle between the incoming wind flow and plane of rotation.

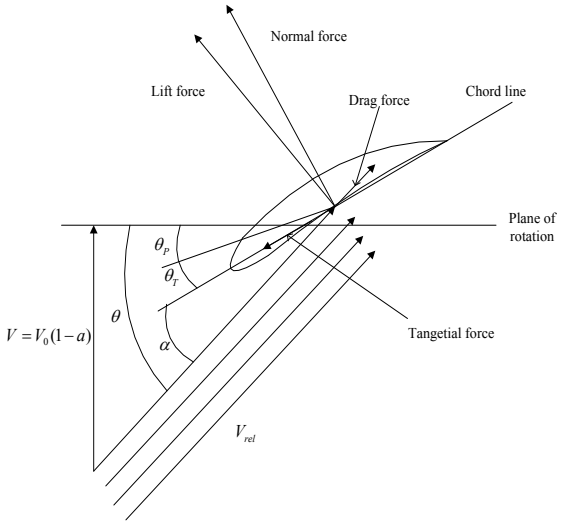

Fig5. Blade element theory geometry

According to virtual work principle, generalized normal force can be expressed as:

$$\begin{aligned} Q_i(x) &= \int_0^L (F_{Lift}\cos(\alpha) + F_{Drag}\sin(\alpha))\phi_r(x)dx \\ &= (F_{Lift}\cos(\alpha) + F_{Drag}\sin(\alpha))\int_0^L \phi_r(x)dx \end{aligned} \qquad (17)$$

where F_{Lift} and F_{drag} is lift force and drag force, α is angle of attack.

2.4 Equation for blade flapwise deflection

The Lagrangian of the blade can be expressed as

$$L = T - V \qquad (18)$$

Substitute kinetic energy, potential energy and aerodynamic forces into Lagrange's equation, the equation that governs the motion of blade flapwise deflection can be expressed as

$$\begin{aligned} &m\mathbf{M}\ddot{\mathbf{q}} + (EI\mathbf{K} + m\omega^2\mathbf{I} - m\omega^2\mathbf{M} \\ &-mg\sin\psi\sin\theta\mathbf{M})\mathbf{q} = \mathbf{Q} + m\dot{\omega}\mathbf{\Phi} \end{aligned} \qquad (19)$$

where $\boldsymbol{Q}$ is the generalized force. The pitch angle has an influence on $\boldsymbol{\emptyset}$, but this effect can only be seen when rotor acceleration is nonzero.

3. INPUT SHAPER DESIGN

Input shaping, which has already successfully used in some mechanical machines, is a method of command filtering that is used to reduce the inducing residual vibration of oscillatory system. We know that an impulse input can excite structural resonance and cause the system to vibrate; however, if we apply a second impulse at a specific time, the residual vibration cause by the first impulse can be reduced or

cancelled. This is the basic idea of input shaping and it is shown in Fig 6.

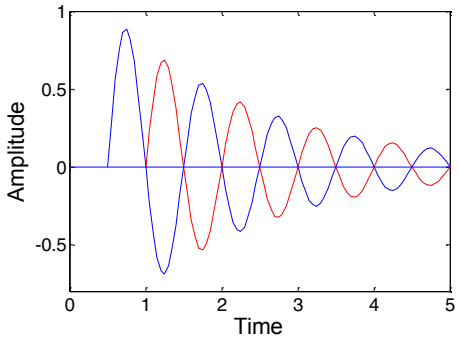

Fig6. Two impulse response

The detailed derivation for the general case of input shaping can be found from reference. Here, we give the equation directly for simplicity.
The amplitude of the residual vibration that results from a sequence of impulses can be described by

$$Amp = \sqrt{\left(\sum_{i=1}^{N} A_i e^{-\zeta\omega(t_N - t_i)} \sin(t_i\omega\sqrt{1-\zeta^2})\right)^2 + \left(\sum_{i=1}^{N} A_i e^{-\zeta\omega(t_N - t_i)} \cos(t_i\omega\sqrt{1-\zeta^2})\right)^2} \quad (20)$$

where A_i is the amplitude of the ith impulse, t_i is the time of the ith impulse. ζ is the damping ratio, ω is the system natural frequency. t_N is the time when the input sequence ends.

Suppression of residual vibration can be obtained by forcing Amp equals to zero, which means the residual vibration is totally eliminated. This is true only when the sine and cosine terms in Amp both equal to zero:

$$\sum_{i=1}^{N} A_i e^{-\zeta\omega(t_N - t_i)} \sin(t_i\omega\sqrt{1-\zeta^2}) = 0 \quad (21)$$

$$\sum_{i=1}^{N} A_i e^{-\zeta\omega(t_N - t_i)} \cos(t_i\omega\sqrt{1-\zeta^2}) = 0 \quad (22)$$

If N impulses are chosen to be the system input, then N terms must be included.

In the input shaper we designed, we use two-impulse input and we assume the first impulse happens at time 0. Also, there is no damping in the model we developed and pitch angle is changed from 15 to 3 degree. With all these conditions, we can solve the above equation,

$$t_{interval} = 0.43835 \quad (23)$$

$$A_1 = A_2 = -6 \quad (24)$$

$t_{interval}$ is the time interval between the two impulses and A_1 and A_2 is the amplitude of the first and second impulse.

To implement the input shaper we designed to our model, we need to change pitch angle from 15 degree to 9 degree first and then change the pitch angle from 9 degree to 3 degree. The second pitch angle change should be happened at 0.43835 seconds later than the first.
To better understand how input shaping works, Fig 7 shows a block diagram of input shaping control scheme with unexpected disturbances. Obviously, the input shaping control is a feedforward control method, uses only the shaped input to control the system.

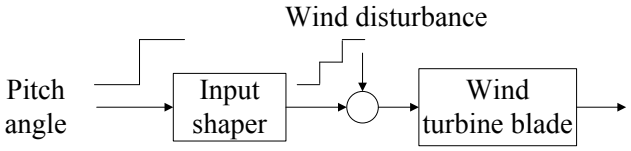

Fig7. Input shaper controller

4. RESULTS AND DISCUSSION

This section provides analysis and discussion about the result we get. More specifically, natural frequency is calculated and centrifugal stiffening's effect on natural frequency is analyzed in this section. Plus, the model we developed is compared with FAST, a CAE tool for horizontal axis wind turbines developed by NREL (National renewable energy laboratory). Also, the effectiveness of designed input shaper is verified by comparison.

4.1 Natural frequency

The natural frequency of the blade is calculated under 3 different wind speed, 0m/s, 8m/s, 18m/s. We choose zero wind speed because we want to see how the natural frequency will behave when there is no rotor speed. The reason why we choose 8m/s and 18m/s is because we'd like to compare the natural frequency when wind turbine is working in region 2 and region 3. Wind turbine has 3 working regions depending on wind speed. In region 2, rotor speed is below rated so the main objective of region 2 control is to capture as much energy as possible. In region 3, wind speed is too high and obtain constant power is the goal of region 3 control.

Table 1 shows the first natural frequencies at different wind speeds. One may observe that the natural frequency increases as the wind speed increases. This is because of the "centrifugal stiffening". When wind speed increases, the rotor speed increase. Meanwhile, the centrifugal force of the blade also increases as a result of increasing rotor speed. This increasing centrifugal force drives the blade from being deformed, making it stiffer. Therefore the natural frequency increases as wind speed increases.

Table 1

Wind speed(m/s)	Natural frequency(radian)	Rotor speed(m/s)
0	7.1273	0
8	7.3693	16.37
18	7.854	69.2

4.2 . Compare with FAST

To see how the model we developed works, we compare it with FAST, a widely used wind turbine analysis software developed by NREL. The wind speed is set to be 18m/s and pitch angle is set to 0. Fig 8 and Fig 9 shows the result we get from our model and FAST when it reaches steady state, from which we can observe that the flapwise deflection in our model is slightly different than that in FAST and the frequency is a little higher than FAST. Several reasons are responsible for the difference. First, we assume blade beam is a uniform beam and use assumed method to calculate flapwise deflection while in FAST the blade is not a uniform beam and finite element method is used to model the blade. There is twist angle in the FAST's blade, which means different section's pitch angle is different. On the contrary, pitch angle in our model is the same all through the blade. Also, parameters used in our model and FAST are different, thus the response get from our model couldn't be the same as that in FAST. Nonetheless, the basic deflection shapes in these two models are similar.

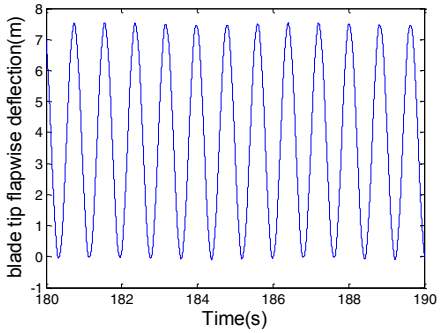

Fig8. Flapwise deflection in our model

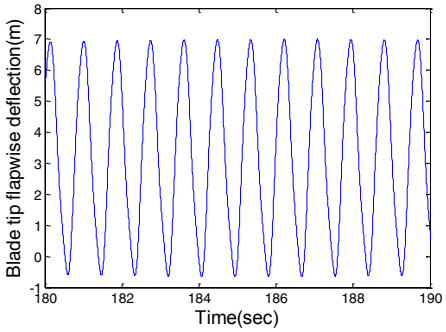

Fig9. Flapwise deflection in FAST

4.3. Input shaping method in reducing vibration

We would like to see how the blade flapwise deflection will react when pitch angle changes. A typical case of this is in region 2, where we need to adjust the pitch angle to the optimal angle so that it can capture as much energy as possible. Therefore, wind speed and rotor speed to are set to 8m/s and 16.37m/s respectively and pitch angle is chosen at two different values, 15 degree and 3 degree. We choose pitch angle to 3 degree is because the optimal pitch angle under the above wind speed and rotor speed is around 3 degree. This conclusion is drawn from the simulation result from WT_Perf. The other pitch angle is just an arbitrary choice different from 3 degree.

Fig 10 shows the flapwise deflection when pitch angle is 15 degree when it reach its steady state and Fig 11 shows the result when pitch angle is 3 degree. As can be observed, the flapwise deflection is worse when the pitch angle is set to 3 degree than it is 15 degree. The reason why this happens is that the wind turbine blade we modeled is pitch-to-feather wind turbine blade.

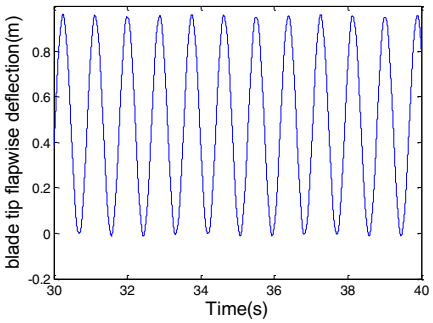

Fig10. Flapwise deflection (pitch angle 15 degree)

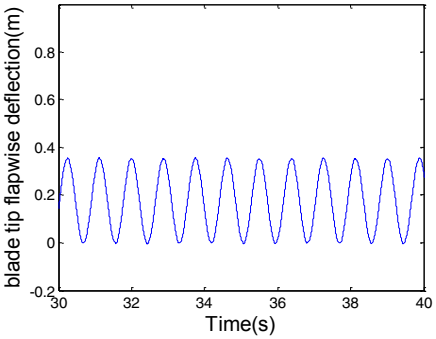

Fig11. Flapwise deflection (pitch angle 3 degree)

To see how pitch angle input will affect the flapwise deflection, we change the pitch from 15 degree to 3 degree at 30 seconds. From Fig 12, it can be seen that some residual vibration is cause since the deflection after 30 seconds is different from when the pitch angle is fixed at 3 degree. The reason why the flapwise deflection cannot return to the steady state when the pitch angle is 3 degree is because there is no damping in the model that we developed.

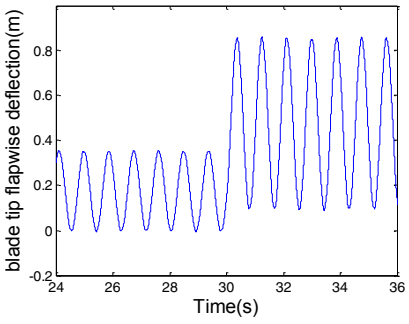

Fig12. Blade flapwise deflection when pitch angle change from 15 degree to 3 degree

Next, we add the input shaper that we design in section 3 to the model and observe the result. For comparison, the response of the system without input shaper and with input shaper is drawn in Fig 13. Clearly, the residual vibration is reduced when input shaping is added to the system, which verifies the effectiveness of input shaper we designed.

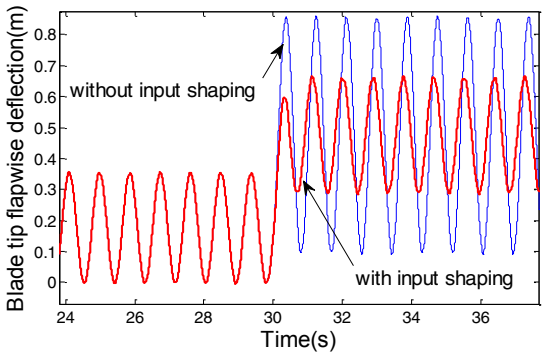

Fig13. Blade flapwise deflection with input shaper

5.CONCLUSION

In this study, the use of input shaper in reducing the blade flapwise vibration has been investigated. First, the model of blade flapwise deflection of wind turbine for vibration analysis purpose is developed using Lagrange's method. When modeling, the blade is treated as cantilever beam with no mass fixed at the top, assumed method is used to calculate the blade flapwise deflection. Centrifugal stiffening is considered in the potential energy when modeling of blade flapwise deflection and its effect on natural frequency is analyzed. When rotor speed increase, the first vibration natural frequency tend to increase as well. Next, input shaper for the model is designed. The effectiveness of designed input shaper is verified by comparing the flapwise deflection with input shaping with the flapwise deflection without input shaping. Although the residual vibration is not zero, there is a good reduction in blade flapwise deflection. Future work is to further refine the model and design a robust input shaper which can tolerate some extent of natural frequency error.

REFERENCES

W. Dixie Dean (2008). Wind turbine mechanical vibrations: Potential environmental threat. *Energy & Environment*. Vol19, 303-307.

Murtagh PJ, Basu B, Broderick BM (2005). Along-wind response of a wind turbine tower with blade coupling subjected to rotationally sampled wind loading. *Engineering Structures*. Vol27, 1209–1219.

Murtagh PJ, Ghosh A, Basu B, Broderick BM (2008). Passive control of wind turbine vibrations including blade/tower interaction and rotationally sampled turbulence. *Wind energy*. Vol11:305-317.

John Arrigan, Vikram Pakrashi, Biswajit Basu, Satish Nagarajaiah (2010). Control of flapwise vibrations in wind turbine blades usin semi-active tuned mass dampers. *Structural control and health monitoring*. Vol18, 840-851

Victor Maldonado, John Farnsworth, William Gressick and Michael Amitay (2010) . Active control of flow separation and structural vibrations of wind turbine blades. *Wind energy*. Vol13,221-237.

Jan-Willem van Wingerden, Anton Hulskamp, Thanasis Barlas, Ivo Houtzager, Harald Bersee, Gijs van Kuik, and Michel Verhaegen (2011). Two-degree-of-freedom active vibration control of a prototyped "smart" rotor. *IEEE transactions on control systems technology*. Vol19,284-296.

Fernando D. Bianchi, Hernán De Battista, Ricardo J. Mantz (2007). *Wind turbine control system:principles, modelling and gain scheduling design*, 16-22. British Library Cataloguing in Publication Data, Britain.

A.R.S. Bramwell, George Done, David Balmford (2001). *Bramwell's Helicopter Dynamics*, 238-246. Butterworth-Heinemann Oxford Aukland New York second edition, USA.

Dana young, Robert P.Felgar, JR (1949). *Tables of characteristic functions representing normal modes of vibration of a beam*. The university of texas publication. USA.

H.P.Lee (1994). Effect of gravity on the stability of a rotating cantilever beam in a vertical plane. *Computers & Structure*. Vol53:351-355.

J.M. Jonkman (2003). *Modeling of the UAE wind turbine for refinement of FAST_AD*. National renewable energy laboratory, 1617 cole Boulevard Golden, Colorado, Master thesis.

Neil Singer, William Singhose, Eric Kriikku (1997). An input shaping controller enabling cranes to move without sway. *American Nuclear Society 7th Topical Meeting on Robotics and Remote Systems*.

N. C. Singer and W. P. Seering (1988). *Preshaping command inputs to reduce system vibration*, 4-8.Massachusetts Institute of Technology, USA.

N. C. Singer (1989). *Residual vibration reduction in computer controlled machines*, 27-30 MIT Artificial Intelligence Laboratory Technical Report Number AITR-1030, MIT Artificial Intelligence Lab.

James M. Hyde (1991). *Multiple mode vibration suppression in controlled flexible systems*, 27-31. MIT Artificial Intelligence Laboratory Technical Report Number 1295, MIT Artificial Intelligence Lab.

David F.Blackburn (2006). *Command shaping for vibration reduction in nonlinear cabled systems*, 2-5. Georgia Institute of Technology, Master thesis.